Frontiers of Physics
https://doi.org/10.1007/s11467-019-0941-0
Front. Phys.
15(2), 23602 (2020)

RESEARCH ARTICLE

# Double Andreev reflections at surface states of the topological insulators with hexagonal warping

**Chang-Yong Zhu[1,2], Shi-Han Zheng[1], Hou-Jian Duan[1], Ming-Xun Deng[1,†], Rui-Qiang Wang[1,‡]**

[1] *Guangdong Provincial Key Laboratory of Quantum Engineering and Quantum Materials, School of Physics and Telecommunication Engineering, South China Normal University, Guangzhou 510006, China*
[2] *School of Physics and Mechanical and Electrical Engineering, Shaoguan University, Shaoguan 512005, China*
*Corresponding authors. E-mail: †dengmingxun@scnu.edu.cn, ‡wangruiqiang@m.scnu.edu.cn*
*Received August 19, 2019; accepted October 20, 2019*

We study the Andreev reflection (AR) at the interface of the topological insulator with hexagonal warping and superconductor junction. Due to the hexagonal warping effect, the double ARs are found in a certain range of the incident angle, where for one incident electron beam, two beams of holes are reflected back. Interestingly, both the beams of holes are reflected as retro-AR on the same side of the normal line of the interface but with different reflection angles, different from the previously reported double AR with one retro-AR and one specular-AR. The double reflections owing to the warping effect show the optics-like property of the Dirac fermion and can stimulate the double reflections of light in anisotropic crystals. In addition, we find that the double ARs are dependent on the hexagonal warping parameter nonmonotonically, and in an intermediate strength the double AR phenomenon is prominent, providing a possibility to explore the warping parameter of topological insulators.

**Keywords** Andreev reflection, topological insulator, warping effect

## 1 Introduction

Andreev reflection (AR) is an important phenomenon of quantum tunneling in normal metal-superconductor (N/S) junctions [1]. At bias voltage below the superconducting gap, the conductance of the N/S junction is mainly determined by the AR processes, where an incident electron from the normal side is reflected as a positive charged hole, possessing the same energy and an opposite spin compared with the incident electron, providing a conversion of electrons into holes [2–5]. In recent years, as plenty of new materials with massless linear excitations are discovered and further used to fabricate N/S interfaces, some novel AR phenomena have been reported [6–10]. According to the reflected directions of holes [11], AR can be classified into retro-AR and specular-AR. For the retro-AR processes, a reflected hole almost retraces the same path of an incident electron and the electron-hole conversion happens usually within intrabands. In contrast, for the specular-AR processes the hole is reflected along a specular path of the incident electron [12–15], where the incident electron and the reflected hole are usually from conduction and valence bands, respectively. For example, Beenakker [12] predicted that a graphene-based N/S junction can exhibit either Andreev retro-AR or specular-AR, depending on the position of Fermi energy. Zhang *et al.* [13] further found that the introduction of the ferromagnetic exchange interaction can suppress the retro-AR but enhance the specular-AR.

Superior to conditional geometrical optics, electronic optics [16, 17] is easy to realize many interesting optics properties, such as negative refraction [18]. A beam of incident electrons is Andreev reflected into two beams of holes, which is similar to the double reflections of light in anisotropic crystals [19, 20]. Double reflection is generally difficult to be achieved in geometrical optics but it is easy in electronic systems [21]. Directions of double reflection in electronic systems are solely determined by the relative orientation of the wavevector and group velocity of the reflected hole, which is in turn determined by the host band structure. When the most works focus on the single AR, it is expected that both retro-AR and specular AR coexist simultaneously for one oblique incident electron in some complex band structure. Recently, Lv and co-workers [11] found that the both retro- and specular-ARs can coexist in a structure with a 2D semiconductor in the presence of a strong Rashba spin–orbit coupling and a d-wave superconductor. The double AR was reported in a type-II Weyl semimetal–superconductor interface, and with the interface changed with respect to the band tilt direction, the double ARs gradually evolve into one retro-AR [22, 23]. In an N/S structure of thin film topological insulator in the presence of a gate electric field, Majidi *et al.* [24] also realized the double ARs within intrabands, where both the incident electron and the reflected hole are from the

same conduction band.

The interplay of the spin–orbit interaction [25] and the superconductivity endow the topological insulator-superconductor (TI/S) junction more interesting physics. The perfect AR has been proposed and discovered in the two dimensional TI/S junction [26]. At low energies, the Dirac cones of helical surface states in three dimensional (3D) TIs are isotropic and appear at top and bottom surfaces [27–29]. When the surface states between top and bottom surface hybridize each other, the reshaped band structure causes the double ARs [24]. If tuning the Fermi energy far away from the Dirac point, the Fermi surface will transform from a circle to a hexagonal snowflake, which is generally called hexagonal warping effect [27, 30] and was observed by the angle-resolved photoemission spectroscopy [31–33]. One can expect that the hexagonal warping Fermi surface will give rise to many unique features, such as electronic transport properties [34–36] and electronic optics [22, 37, 38]. For instance, in a hexagonally warped TI/N junction, an incident electron beam can lead to two reflection states propagating along different directions [21] and the double refraction [39].

In this paper, we extend the primary study [21] to consider the effect of hexagonal warping on Andreev reflections in a TI/S junction. We show that the hexagonal warping Fermi surface can lead to double AR as well as double normal reflection (NR). Interestingly, both the reflected two holes are reflected as retro-AR on the same side of the normal line of the interface with different reflection angles, different from the previously reported double ARs with one retro-AR and one specular-AR, where one hole inhabits at the same side and the other at the opposite side of incident electrons, respectively. The outline of the paper is as follows. In Section 2, we introduce our model and the formalisms which will be used for the reflection probability computation. In Section 3, we present our numerical results for the probabilities of the double normal electron and double Andreev reflections and discuss the effect of hexagonal warping parameter on the reflection processes. Finally, we give a conclusion of our work in Section 4.

## 2 Model and theory

Our system is a TI/S hybrid structure on the surface of a 3D TI, as shown in Fig. 1(a), where the superconductivity is induced via the proximity effect by depositing superconductor. The proximity-induced superconductivity has been extensively demonstrated in 3D TIs [40–45] based on $Bi_2Se_3$. The TI/S interface is located at the $x = 0$ plane, with $x < 0$ the topological insulator (TI region) and $x > 0$ the superconductor (S region). Electron transport is along the $x$ axis. The scattering at the TI/S interface for quasiparticles is described by the Bogoliubov–de Gennes (BdG) equations [2, 4]:

$$\begin{pmatrix} H_0(\boldsymbol{k}) - \mu & \Delta(\boldsymbol{r}) \\ -\Delta^*(\boldsymbol{r}) & \mu - H_0^*(-\boldsymbol{k}) \end{pmatrix} \psi = E\psi. \quad (1)$$

Here, we assume the S side is of the conventional s-wave superconductor. $\psi = (\psi_\uparrow, \psi_\downarrow, \psi_\uparrow^*, \psi_\downarrow^*)^T$ is a four-component spinor wave function, whose upper two components correspond to electron spinor and lower two components correspond to hole spinor. $\Delta(\boldsymbol{r}) = \mathrm{i}\sigma_y\Delta_0\Theta(x)$ represents the superconducting pairing potential with $\Theta(x)$ the Heaviside step function and $\boldsymbol{\sigma} = (\sigma_x, \sigma_y, \sigma_z)$ the Pauli matrix in real spin space. $\mu$ is the chemical potential of the whole system and $E$ is the quasiparticle excitation energy measured from the Fermi level. $H_0$ is the Hamiltonian of the TI surface state with the hexagonal warping, which is generally expressed as [21, 27]

$$H_0(\boldsymbol{k}) = v(k_x\sigma_y - k_y\sigma_x) + \frac{\lambda}{2}(k_+^3 + k_-^3)\sigma_z + V(\boldsymbol{r}). \quad (2)$$

Here $k_\pm = k_y \pm \mathrm{i}k_x$; $v$ and $\lambda$ denote Fermi velocity and hexagonal warping parameter, respectively; $V(\boldsymbol{r}) = -U\Theta(x)$ is the electrostatic potential exerting on different regions. In above Hamiltonian of Eq. (2), the term breaking particle-hole symmetry is discarded since it has negligible effect for Andreev reflection under consideration. By introducing a characteristic length scale $a = \sqrt{\lambda/v}$ and a characteristic energy scale $E_w = \sqrt{v^3/\lambda}$, one can rewrite the Hamiltonian (2) to be

$$H_0' = \left[(q_x\sigma_y - q_y\sigma_x) + \frac{1}{2}(q_+^3 + q_-^3)\sigma_z\right] E_w + V(\boldsymbol{r}), \quad (3)$$

where $\boldsymbol{q} = \boldsymbol{k}a$ is a dimensionless parameter wave vector. The warping effect is completely encoded in $E_w$, which is convenient to distinguish the warping dominant region ($\mu > E_w$) from the warping negligible region ($\mu < E_w$).

By solving the BdG equation, we can obtain the energy dispersions for electron and hole excitations in the TI region,

$$E_{e\pm}(\boldsymbol{q}) = \pm\sqrt{q^2 + q_y^2(q_y^2 - 3q_x^2)^2}E_w - \mu, \quad (4)$$

$$E_{h\pm}(\boldsymbol{q}) = \pm\sqrt{q^2 + q_y^2(q_y^2 - 3q_x^2)^2}E_w + \mu, \quad (5)$$

with $q^2 = q_x^2 + q_y^2$. $E_{e+}$ and $E_{h-}$ are, respectively, the conduction bands for electron and hole, while $E_{e-}$ and $E_{h+}$ are their valence bands. In the S region, the excitation energy is

$$E_s(q) = \sqrt{\left(\widetilde{U} \pm \sqrt{q^2 + q_y^2(q_y^2 - 3q_x^2)^2}E_w\right)^2 + \Delta^2}, \quad (6)$$

where $\widetilde{U} = \mu + U$.

Our discussion is limited to the conduction band and we are interested in the high energy region (i.e., $\mu > E_w$) where the warping effect plays an important role. In

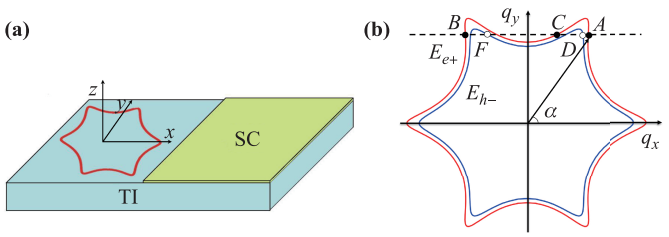


**Fig. 1** **(a)** Schematic illustration of TI/S junction with the hexagonal warping on surface of TIs. **(b)** Snowflake equal-energy surfaces in the $q_x$–$q_y$ plane in the TI side with hexagonal warping. The conducting band for electrons (holes) is colored with red line (blue line). Point $A$ is the incident electron mode with an incident angle $\alpha$, and points $B$–$C$ and points $D$–$F$ are the normally reflected electron modes and Andreev reflected hole modes, respectively.

Fig. 1(b), we plot the snowflake-shaped equienergy surfaces (Fermi surfaces) in the $q_x$–$q_y$ plane for finite $\mu > 0$ in the TI side with hexagonal warping, where the red line denotes for the electron conduction band $E_{e+}$ and the blue line for hole conduction band $E_{h-}$. When an electron is incident along $x$-axis, the energy $E$ and the wave vector $q_y$ remain invariant. Since $E_{e(h)}(\boldsymbol{q})$ contains a quadratic term of $q_x$, there are two solutions of $q_x$ in equation $E_{e(h)}(\boldsymbol{q}) = E$ for electrons and two solutions for holes. When an electron is incident with angle $\alpha = q_y/q_x$ from point $A$, the wave vectors at the points $B$ and $C$ are the normally reflected electron modes while those at points $D$ and $F$ are Andreev reflected hole modes. Thus, the double Andreev reflection and double normally reflection would be expected.

In order to explore this interesting double Andreev reflection, we further calculate the transport properties of the scattering. We denote the amplitudes of the double normal electron reflections as $r_B^e$ and $r_C^e$ and those of the double AR reflections as $r_D^h$ and $r_F^h$. The wave function in the TI region can be expressed as

$$\psi_N(r) = \psi_{e,A} + r_B^e\psi_{e,B} + r_C^e\psi_{e,C} + r_D^h\psi_{h,D} + r_F^h\psi_{h,F}, \quad (7)$$

where

$$\psi_{e,A} = \begin{pmatrix} 1 \\ u_A \\ 0 \\ 0 \end{pmatrix} e^{i(q_{A,x}x+q_y y)}, \quad \psi_{e,B} = \begin{pmatrix} 1 \\ u_B \\ 0 \\ 0 \end{pmatrix} e^{i(q_{B,x}x+q_y y)},$$

$$\psi_{e,C} = \begin{pmatrix} 1 \\ u_C \\ 0 \\ 0 \end{pmatrix} e^{i(q_{C,x}x+q_y y)}, \quad \psi_{h,D} = \begin{pmatrix} 0 \\ 0 \\ 1 \\ v_D \end{pmatrix} e^{i(q_{D,x}x+q_y y)},$$

$$\psi_{h,F} = \begin{pmatrix} 0 \\ 0 \\ 1 \\ v_F \end{pmatrix} e^{i(q_{F,x}x+q_y y)}.$$

Here,

$$u_m = \frac{q_y(q_y^2 - 3q_{m,x}^2)E_w - \mu - E}{(iq_{m,x} + q_y)E_w} \text{ for } m = \{A, B, C\},$$

$$v_n = \frac{q_y(q_y^2 - 3q_{n,x}^2)E_w - \mu + E}{(iq_{n,x} + q_y)E_w} \text{ for } n = \{D, F\},$$

and

$$q_{A,x} = -q_{B,x} = \frac{1}{3\sqrt{2q_y^2}}\sqrt{\eta + \zeta_+},$$

$$q_{C,x} = \frac{1}{3\sqrt{2q_y^2}}\sqrt{\eta - \zeta_+},$$

$$q_{D,x} = \frac{1}{3\sqrt{2q_y^2}}\sqrt{\eta + \zeta_-},$$

$$q_{F,x} = -\frac{1}{3\sqrt{2q_y^2}}\sqrt{\eta - \zeta_-}.$$

with $\eta = 6q_y^4 - 1$ and $\zeta_\pm = \sqrt{1 + \frac{36q_y^2}{E_w^2}(\mu \pm E)^2 - 48q_y^4}$.

In the S region, the total outgoing wave function is the superposition of two electron-like and two hole-like quasiparticle states,

$$\psi_S(r) = \sum_{j=1}^{4} t_j \begin{pmatrix} M_j\Delta \\ 2M_{2j}\Delta\widetilde{U} \\ M_{2j}[M_j - 2\widetilde{U}(M_{1j} + \widetilde{U} + E)] \\ -M_j(M_{1j} - \widetilde{U} - E) - 2\widetilde{U}M_{2j}M_{3j} \end{pmatrix} e^{i(q_{s,j}x+q_y y)}, \quad (8)$$

where the longitudinal wave vectors $q_{s,j}$ is the solution of $q_x$ to the equation $E = \sqrt{\left(\widetilde{U} \pm \sqrt{q^2 + q_y^2(q_y^2 - 3q_x^2)^2}E_w\right)^2 + \Delta^2}$. The other quantities are defined as $M_{1j} = q_y(q_y^2 - 3q_{s,j}^2)E_w$, $M_{2j} = (iq_{s,j} + q_y)E_w$, $M_{3j} = (-iq_{s,j} + q_y)E_w$, and $M_j = (M_{1j} + \widetilde{U})^2 + M_{2j}M_{3j} + \Delta_0^2 - E^2$. The coefficients $t_j$ with $j = 1, 2, 3, 4$ of Eq. (8) describe the amplitudes of the quasiparticles in the superconductor region. They are determined by matching the boundary conditions at the interface: $\psi_N|_{x=0^-} = \psi_S|_{x=0^+}$ and $\frac{\partial\psi_N}{\partial x}|_{x=0^-} = \frac{\partial\psi_S}{\partial x}|_{x=0^+}$.

The particle current density operator in the TI region can be derived via $J = \frac{-i}{\hbar}[\boldsymbol{r}, H_{BdG}]$, where $H_{BdG} = diag\{H_0'(\boldsymbol{q})-\mu, \mu-H_0'^*(-\boldsymbol{q})\}$. The $x$-component of current density is $J_x = (\tau_z\sigma_y - 6q_xq_y\tau_0\sigma_z)E_w$, where $\tau_z$ and $\tau_0$ are the $z$-component of Pauli matrix and identity matrix in particle-hole space, respectively. Finally, the double NR coefficients $R_B^e$ and $R_C^e$ and the double AR coefficients $R_D^h$ and $R_F^h$ can be calculated through [22]

$$R_i^e = \left|\frac{\langle\psi_{e,i}|\, J_x\, |\psi_{e,i}\rangle}{\langle\psi_{e,A}|\, J_x\, |\psi_{e,A}\rangle}\right| |r_i^e|^2, \quad i = \{B, C\}, \tag{9}$$

$$R_l^h = \left|\frac{\langle\psi_{h,l}|\, J_x\, |\psi_{h,l}\rangle}{\langle\psi_{e,A}|\, J_x\, |\psi_{e,A}\rangle}\right| |r_l^h|^2, \quad l = \{D, F\}. \tag{10}$$

## 3 Numerical results and discussion

In the following numerical calculations, we set the typical parameters [27, 34]: $v = 0.25$ eV·nm, $\lambda = 0.25$ eV·nm$^3$, $\Delta = 0.01$ eV, and $U = 30$ eV, and the incident energy $E = 0.5\Delta$ of an electron unless otherwise statement. Firstly, we consider the low energy case with $\mu = 0.05$ eV, where the hexagonal warping be ignored. In this situation, there exist only a single NR and a single AR, as shown by the dispersion $E(\boldsymbol{q})$ along $q_x$ direction in Fig. 2(b), where the red solid line stands for the conducting band of electrons $E_{e+}$ and the blue dashed line for holes $E_{h-}$. Point $A$ is the incident electron mode, and points $B$ and $D$ are the NR electron mode and AR hole mode, respectively. The corresponding schematic diagram is illustrated in Fig. 2(c), where the incident and reflection angles are almost strictly equal due to the isotropic Fermion surface. The probability of the normal and Andreev reflection processes as a function of the incident angle $\alpha$ are plotted in Fig. 2(a). With the incident angle increasing from $\alpha = 0$ to $\pi/2$, the AR probability $R_D^h$ decays from perfect unit at the normal incidence, after a critical angle, down to zero while the NR probability exhibits a opposite behavior. At intermediate certain angle, they reach equal. The Fermi surface of TI surface states at low energy is a circle and thus for an incident electron, there exist only a single NR and a single AR mode, which is a typical behavior of the isotropic scattering. However, when the Fermi surface is hexagonally warped, which can be obtained by tuning Fermi energy away from the Dirac point, an incident electron beam will present more reflection states propagating along different directions as following discussions.

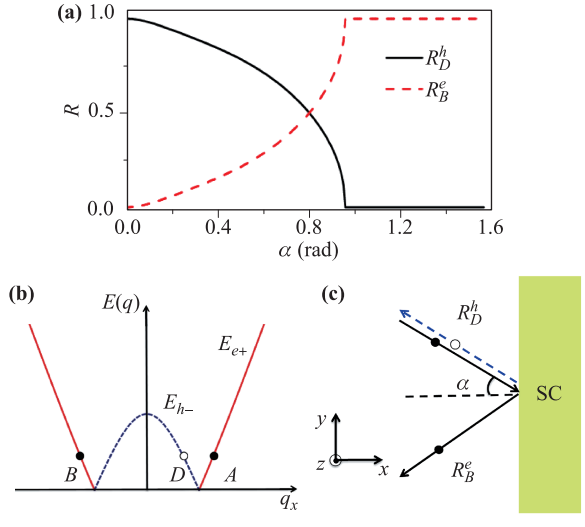


**Fig. 2** **(a)** The normal and Andreev reflection probabilities as a function of incident angle $\alpha$ (in unit of rad) in low energy regime $\mu = 0.05$ eV, where the hexagonal warping is negligible. **(b)** Dispersion of conducting band (red solid line) for electrons $E_{e+}$ and holes $E_{h-}$ (blue dashed line) versus $q_x$ with finite $q_y$. Point $A$ is the incident electron mode, and points $B$ and $D$ are the NR electronmode and AR hole mode, respectively. **(c)** The corresponding schematic diagram of a single NR and a single AR, where the incident and reflected angles are equal. The other parameter is $U = 0.5$ eV.

For high energy with $\mu = 1.3$ eV, the hexagonal warping of topological insulator plays a role in scattering processes. Owing to the snowflake shape of Fermi surface, there are more scattering processes. In order to clarify it, we plot the dispersions $E_{e+}$ and $E_{h-}$ along $q_x$ direction in Fig. 3(b) for finite $q_y$, corresponding to the horizontal dashed line in Fig. 1(b). When an electron is incident with angle $\alpha = q_y/q_x$ from point $A$, besides the NR at point $B$ and AR at point $D$, there emerge additional one AR and one NR, located at points $C$ and $F$, respectively. In Fig. 3(a), we present the behavior of the probability of double NRs and double ARs as a function of the incident angle $\alpha$. For $\alpha = 0$, $R_D^h = 1$ and the others are zero, and this scenario is the same as Fig. 2(a). With the incident angle slightly deviating from the normal incident direction, the probability of the electron–hole conversion $R_D^h$ decreases sharply to a stable value while the normal reflection probability $R_B^e$ sharply increases, exceeding $R_D^h$. Compared with Fig. 2(a), warping parameter $\lambda$ can sensitively suppress AR $R_D^h$ and support $R_B^e$, whose evolution with $\alpha$ is illustrated in inset of Fig. 3(a). This is a consequence of the large momentum mismatch of of Cooper pairs $(\boldsymbol{k}_A, \boldsymbol{k}_D)$ under the hexagonal structure on the equal-energy surface. With the incident angle increase further, both the probability of the Andreev reflection probability $R_D^h$ and the normal reflection probability $R_B^e$ almost remain a stable plateau until a large $\alpha$. Close to $\alpha = \pi/3$, both $R_D^h$ and $R_B^e$ decrease quickly. Interestingly, accompanied with this, there emerge a new Andreev reflection $R_F^h$ from the point $F$ and a new NR $R_C^e$ from the point $C$. The new normal reflection $R_C^e$ takes the place of $R_B^e$, increasing up to the maximum. Thus, in the vicinity of the incident angle $\alpha = \pi/3$, there emerge double NRs and ARs. All $\pm x$-moving modes are either propagating states or evanescent states depending on whether $q_x$ is real or imaginary. According to this, the crucial angle of double NR and AR are determined by $\pi/3 > \alpha > \arcsin(|\boldsymbol{k}_D|/|\boldsymbol{k}_A|)$, within

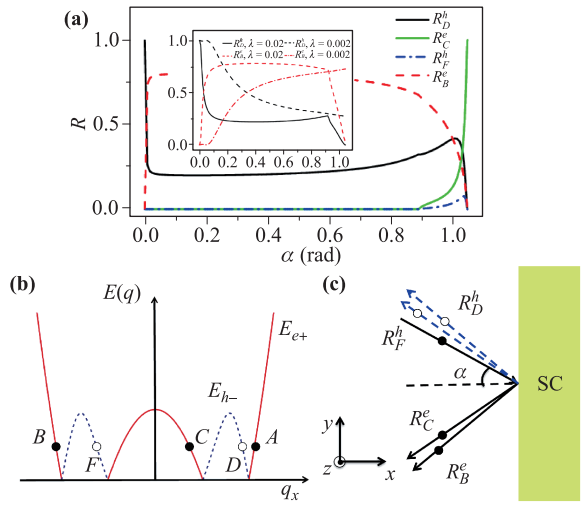


**Fig. 3** **(a)** The probabilities of the double normal ($R^e_B$ and $R^e_C$) and double Andreev ($R^h_D$ and $R^h_F$) reflections as a function of the incident angle $\alpha$ (in unit of rad) in high energy regime $\mu = 1.3$ eV. The inset shows the evolution of all the reflected probabilities with warping parameters $\lambda$ (in unit of eV nm$^3$). **(b)** Dispersion of conducting band (red solid line) for electrons $E_{e+}$ and holes (blue dashed line) $E_{h-}$ via $q_x$ with finite $q_y$. Point $A$ is the incident electron mode, $B$–$C$ and $D$–$F$ are the normally reflected electron modes and Andreev reflected hole modes, respectively. **(c)** The schematic diagram of double NRs and double ARs.

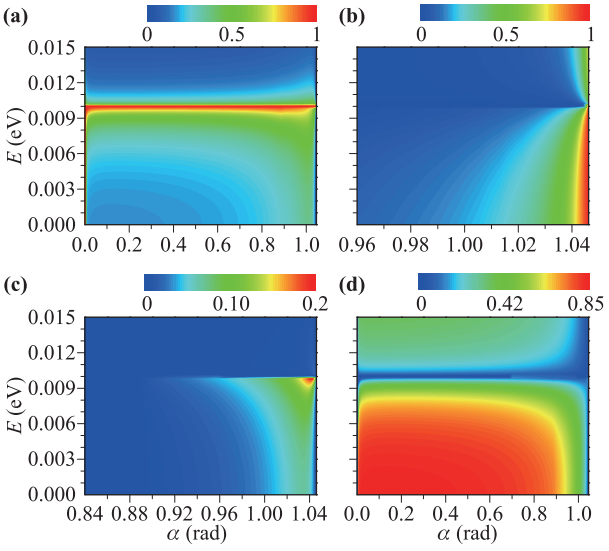


**Fig. 4** The incident angle $\alpha$ and energy dependence $E$ of **(a)** AR $R^h_D$, **(b)** NR $R^e_C$, **(c)** AR $R^h_F$, and **(d)** NR $R^e_B$, respectively.

which $\boldsymbol{k}^e_B$, $\boldsymbol{k}^h_D$, and $\boldsymbol{k}^h_F$ vanish completely and only $R^e_C$ survives. Double reflection generally cannot be achieved in optics and thus is unique in electronic optics.

An incident electron of the conduction band from the left to the N/S interface, with a subgap energy, can be either retro or specularly reflected as a hole (or an electron). In order to classify these reflections, we can inspect the relative orientation of the wave vector and group velocity of the reflected holes (or electrons). We find that the product of wave vector and group velocity for the electron at point $B(C)$, $\boldsymbol{q}_i \cdot \boldsymbol{v}_{g,i} = \frac{[q^2+3(q^3\sin 3\alpha_i)^2]E_w}{\sqrt{q^2+(q^3\sin 3\alpha_i)^2}} > 0$, has the same sign as that of the incident electron at point $A$. Thus, both NRs are specular reflected electrons, which lie at the opposite side with respect to the incident direction. For the hole at point $D(F)$, the reflected holes, $\boldsymbol{q}_i \cdot \boldsymbol{v}_{g,i} = -\frac{[q^2+3(q^3\sin 3\alpha_i)^2]E_w}{\sqrt{q^2+(q^3\sin 3\alpha_i)^2}} < 0$, has the opposite sign as that of the incident electron. Therefore, both the reflections with the wave vector at points $D$ and $F$ are retro-ARs, which lie at the same side with respect to the incident direction. The schematic diagram is illustrated in Fig. 3(c). Although both ARs or NRs inhabit at the same side, their reflection angles are not same and also not equal to the incident angle due to the difference of momentum at each point. One can recall that the double ARs are also presented in TI thin film [24], where the upper-bottom surface coupling is considered, and in type-II Weyl semimetal [22] where two Weyl points coupling are taken into account. Here, the double ARs emerge owing to the surface warping effect, completely different from previous mechanisms. Double reflection generally cannot be achieved in optics and thus is unique in electronic optics. This phenomenon provides an opportunity to simulate the double reflections of light in anisotropic crystals and also to explore the warping strength of TIs.

From above discussions, one can see that the scattering processes are not only sensitive to the incident angle $\alpha$, but also the incident energy $E$. We plot the dependence of the double NR and AR coefficients on the incident energy and angle in Fig. 4, where Figs. 4(a)–(d) correspond to $R^h_D, R^e_C, R^h_F$ and $R^e_B$, respectively. It is shown that the AR $R^h_D$ and $R^h_F$ decay quickly to zero out of the superconductor gap $E > \Delta$. The probability $R^h_D$ is large with nearly unit probability when the energy $E$ reaches the superconductor gap, almost independent of the incident

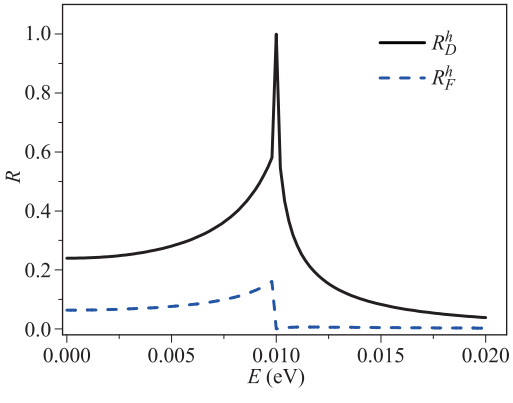


**Fig. 5** The double ARs $R^h_D$ and $R^h_F$ as a function of the incident energy $E$ for large incident angle $\alpha = 1.035$ rad.

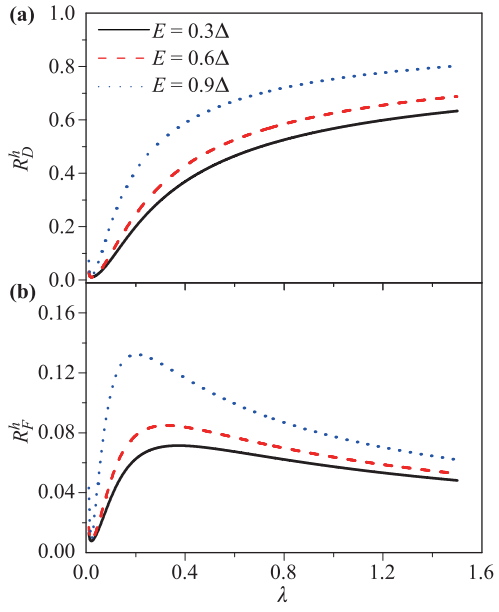


**Fig. 6** The double Andreev reflections **(a)** $R_D^h$ and **(b)** $R_F^h$ as a function of warping parameter $\lambda$ (in unit of eV nm$^3$) with fixed $\alpha = 1.035$ rad, for different incident energies $E$.

angle $\alpha$, as shown in Fig. 4(a). Similar AR is found in Ref. [24]. Figure 4(c) shows that the AR $R_F^h$ from the point $F$ occurs mainly in the region of large incident angle and increases with the incident energy $E$. Compared Figs. 4(b) and (d), $R_B^e$ at a large incident angle is replaced by $R_C^e$ with unit probability. At the large incident angle $\alpha$, though the AR $R_F^h$ is smaller than $R_D^h$, it can be visible. Dependence of $R_F^h$ and $R_D^h$ on the incident energy $E$ for $\alpha$ slightly below $\pi/3$ is illustrated in Fig. 5.

Figures 6(a) and (b) show the warping parameter $\lambda$ dependence of the double AR probability $R_D^h$ and $R_F^h$ for different values of incident energy $E$ with $\alpha = 1.035$ rad. It is found that the dependence of the probability $R_D^h$ on $\lambda$ is monotonously increasing, while the probability $R_F^h$ first increases with $\lambda$ and then decreases by increasing $\lambda$. At an appropriate $\lambda$, the double ARs are most prominent.

## 4 Conclusion

In conclusion, we have studied the Andreev reflection at the TI/S junction on the surface of a 3D TI with the hexagonal warping. Different usual circle Fermi surface, the hexagonal shape supports four scattering processes– double Andreev reflections together with double normal electron reflections in a certain range of the incident angle. Appearance of the double ARs, attributed to the hexagonal warping effect of surface states of TIs, is completely different from previously reported mechanisms. Interestingly, both the reflected holes are reflected as retro-AR with different reflection angles. Compared with the previously reported double ARs with one retro-AR and one specular-AR, where one hole inhabits at the same side of incident electrons and the other at the opposite side, the double reflections from the warping effect is more suitable to stimulate the double reflections of light in anisotropic crystals. We also have studied the effect of warping parameter $\lambda$ on the double AR probability, and find that in intermediate strength of $\lambda$, the double AR phenomenon is the most prominent, suitable for the experiment observation.

**Acknowledgements** This work was supported by GDUPS (2017), the National Natural Science Foundation of China (Grant Nos. 11874016, 11474106, and 11904107), and the Key Program for Guangdong NSF of China (Grant No. 2017B030311003).

## References

1. A. F. Andreev, The thermal conductivity of the intermediate state in superconductors, *Sov. Phys. JETP* 19(5), 1228 (1964) [*Zh. Eksp. Teor. Fiz.* 46, 1823(1964)]
2. P. G. de Gennes, in: Superconductivity of Metals and Alloys, Benjamin, New York, 1966
3. J. Linder and J. W. A. Robinson, Superconducting spintronics, *Nat. Phys.* 11(4), 307 (2015)
4. G. E. Blonder, M. Tinkham, and T. M. Klapwijk, Transition from metallic to tunneling regimes in superconducting microconstrictions: Excess current, charge imbalance, and supercurrent conversion, *Phys. Rev. B* 25(7), 4515 (1982)
5. P. Lv, A. M. Guo, H. Y. Li, C. X. Liu, X. C. Xie, and Q. F. Sun, Spin-flip reflection at the normal metal-spin superconductor interface, *Phys. Rev. B* 95(10), 104516 (2017)
6. C. W. J. Beenakker, Andreev reflection and Klein tunneling in graphene, *Rev. Mod. Phys.* 80(4), 1337 (2008)
7. K. K. Li and Y. Y. Zhang, Spin-filtered and spatially distinguishable crossed Andreev reflection in a silicene-superconductor junction, *Phys. Rev. B* 94(16), 165441 (2016)
8. C. X. Bai, Y. L. Yang, and X. D. Zhang, Specular Andreev reflection and magnetoresistance in graphene-based ferromagnet-superconductor double junctions, *Appl. Phys. Lett.* 92(10), 102513 (2008)
9. R. Q. Wang, L. Sheng, L. B. Hu, M. Yang, B. G. Wang, and D. Y. Xing, Generation of adjustable pure spin currents in negative-U systems, *Front. Phys.* 9(4), 477 (2014)
10. Z. M. Yu, Y. Liu, and S. A. Yang, Anomalous spatial shifts in interface electronic scattering, *Front. Phys.* 14(3), 33402 (2019)
11. B. Lv, C. Zhang, and Z. Ma, Specular Andreev reflection in the interface of a two-dimensional semiconductor with Rashba spin-orbit coupling and a d-wave superconductor, *Phys. Rev. Lett.* 108(7), 077002 (2012)
12. C. W. J. Beenakker, Specular Andreev reflection in graphene, *Phys. Rev. Lett.* 97(6), 067007 (2006)

13. Q. Y. Zhang, D. Y. Fu, B. G. Wang, R. Zhang, and D. Y. Xing, Signals for specular Andreev reflection, *Phys. Rev. Lett.* 101(4), 047005 (2008)
14. D. K. Efetov, L. Wang, C. Handschin, K. B. Efetov, J. Shuang, R. Cava, T. Taniguchi, K. Watanabe, J. Hone, C. R. Dean, and P. Kim, Specular interband Andreev reflections at van der Waals interfaces between graphene and $NbSe_2$, *Nat. Phys.* 12(4), 328 (2016)
15. S. G. Cheng, Y. Xing, J. Wang, and Q. F. Sun, Controllable Andreev retroreflection and specular Andreev reflection in a four-terminal graphene-superconductor hybrid system, *Phys. Rev. Lett.* 103(16), 167003 (2009)
16. V. V. Cheianov, V. Fal'ko, and B. L. Altshuler, The focusing of electron flow and a Veselago lens in graphene p-n junctions, *Science* 315(5816), 1252 (2007)
17. S. Li, C. Wang, S. H. Zheng, R. Q. Wang, J. Li, and M. Yang, Dynamic conductivity modified by impurity resonant states in doping three-dimensional Dirac semimetals, *Front. Phys.* 13(2), 137303 (2018)
18. F. Hassler, A. R. Akhmerov, and C. W. J. Beenakker, Flat-lens focusing of electrons on the surface of a topological insulator, *Phys. Rev. B* 82(12), 125423 (2010)
19. H. Ren, L. Liu, D. Liu, and Z. Song, Double refraction and reflection of sequential crystal interfaces with arbitrary orientation of the optic axis and application to optimum design, *J. Mod. Opt.* 52(4), 529 (2005)
20. J. F. Wu and C. M. Zhang, The double reflection on the interface of uniaxial crystals in the Savart polariscope, *Sci. China Ser. G-Phys. Mech. Astron.* 52(7), 1003 (2009)
21. Z. M. Yu, D. S. Ma, H. Pan, and Y. G. Yao, Double reflection and tunneling resonance in a topological insulator: Towards the quantification of warping strength by transport, *Phys. Rev. B* 96(12), 125152 (2017)
22. Z. Hou and Q. F. Sun, Double Andreev reflections in type-II Weyl semimetal-superconductor junctions, *Phys. Rev. B* 96(15), 155305 (2017)
23. X. S. Li, S. F. Zhang, X. R. Sun, and W. J. Gong, Double Andreev reflections and double electron transmissions in a normal-superconductor-normal junction based on type-II Weyl semimetal, *New J. Phys.* 20(10), 103005 (2018)
24. L. Majidi and R. Asgari, Specular Andreev reflection in thin films of topological insulators, *Phys. Rev. B* 93(19), 195404 (2016)
25. X. S. Li, C. Wang, M. X. Deng, H. J. Duan, P. H. Fu, R. Q. Wang, L. Sheng, and D. Y. Xing, Photoninduced Weyl half-metal phase and spin filter effect from topological Dirac semimetals, arxiv: 1910.06178 (2019)
26. I. Knez, R. R. Du, and G. Sullivan, Andreev reflection of helical edge modes in InAs/GaSb quantum spin Hall insulator, *Phys. Rev. Lett.* 109(18), 186603 (2012)
27. L. Fu, Hexagonal warping effects in the surface states of the topological insulator $Bi_2Te_3$, *Phys. Rev. Lett.* 103(26), 266801 (2009)
28. M. Z. Hasan and C. L. Kane, Topological insulators, *Mod. Phys.* 82(4), 3045 (2010)
29. X. L. Qi and S. C. Zhang, Topological insulators and superconductors, *Rev. Mod. Phys.* 83(4), 1057 (2011)
30. S. Souma, K. Kosaka, T. Sato, M. Komatsu, A. Takayama, T. Takahashi, M. Kriener, K. Segawa, and Y. Ando, Direct measurement of the out-of-plane spin texture in the Dirac-cone surface state of a topological insulator, *Phys. Rev. Lett.* 106(21), 216803 (2011)
M. Nomura, S. Souma, A. Takayama, T. Sato, T. Takahashi, K. Eto, K. Segawa, and Y. Ando, Relationship between Fermi surface warping and out-of-plane spin polarization in topological insulators: A view from spin- and angle-resolved photoemission, *Phys. Rev. B* 89(4), 045134 (2014)
31. Y. Xia, D. Qian, D. Hsieh, L. Wray, A. Pal, H. Lin, A. Bansil, D. Grauer, Y. S. Hor, R. J. Cava, and M. Z. Hasan, Observation of a large-gap topological-insulator class with a single Dirac cone on the surface, *Nat. Phys.* 5(6), 398 (2009)
32. Y. L. Chen, J. G. Analytis, J. H. Chu, Z. K. Liu, S. K. Mo, X. L. Qi, H. J. Zhang, D. H. Lu, X. Dai, Z. Fang, S. C. Zhang, I. R. Fisher, Z. Hussain, and Z. X. Shen, Experimental realization of a three-dimensional topological insulator, $Bi_2Te_3$, *Science* 325(5937), 178 (2009)
33. K. Kuroda, M. Ye, A. Kimura, S. V. Eremeev, E. E. Krasovskii, E. V. Chulkov, Y. Ueda, K. Miyamoto, T. Okuda, K. Shimada, H. Namatame, and M. Taniguchi, Experimental realization of a three-dimensional topological insulator phase in ternary chalcogenide $TlBiSe_2$, *Phys. Rev. Lett.* 105(14), 146801 (2010)
34. Z. Li and J. P. Carbotte, Hexagonal warping on spin texture, Hall conductivity, and circular dichroism of topological insulators, *Phys. Rev. B* 89(16), 165420 (2014)
35. S. Roy, A. Soori, and S. Das, Tunnel magnetoresistance scan of a pristine three-dimensional topological insulator, *Phys. Rev. B* 91(4), 041109 (2015)
36. Z. B. Siu, M. B. Jalil, and S. G. Tan, Topological state transport in topological insulators under the influence of hexagonal warping and exchange coupling to in-plane magnetizations, *Sci. Rep.* 4(1), 5062 (2015)
37. F. Hassler, A. R. Akhmerov, and C. W. J. Beenakker, Flat-lens focusing of electrons on the surface of a topological insulator, *Phys. Rev. B* 82(12), 125423 (2010)
38. T. Habe and M. Koshino, Spin-dependent refraction at the atomic step of transition-metal dichalcogenides, *Phys. Rev. B* 91(20), 201407 (2015)
39. P. Lv, N. Dai, and Q. F. Sun, Double refraction and spin splitter in normal-conductor/hexagonal-semiconductor junctions, *Phys. Rev. B* 97(23), 235425 (2018)
40. D. Zhang, J. Wang, A. M. DaSilva, J. S. Lee, H. R. Gutierrez, M. H. W. Chan, J. Jain, and N. Samarth, Superconducting proximity effect and possible evidence for Pearl vortices in a candidate topological insulator, *Phys. Rev. B* 84(16), 165120 (2011)
41. M. X. Wang, C. Liu, J. P. Xu, F. Yang, L. Miao, M. Y. Yao, C. L. Gao, C. Shen, X. Ma, X. Chen, Z. A. Xu, Y. Liu, S. C. Zhang, D. Qian, J. F. Jia, and Q. K. Xue, The coexistence of superconductivity and topological order in the $Bi_2Se_3$ thin films, *Science* 336(6077), 52 (2012)

42. J. R. Williams, A. J. Bestwick, P. Gallagher, S. S. Hong, Y. Cui, A. S. Bleich, J. G. Analytis, I. R. Fisher, and D. Goldhaber-Gordon, Unconventional Josephson effect in hybrid superconductor-topological insulator devices, *Phys. Rev. Lett.* 109(5), 056803 (2012)

43. L. Galletti, S. Charpentier, M. Iavarone, P. Lucignano, D. Massarotti, R. Arpaia, Y. Suzuki, K. Kadowaki, T. Bauch, A. Tagliacozzo, F. Tafuri, and F. Lombardi, Influence of topological edge states on the properties of $Al/Bi_2Se_3/Al$ hybrid Josephson devices, *Phys. Rev. B* 89(13), 134512 (2014)

44. E. S. Tikhonov, D. V. Shovkun, M. Snelder, M. P. Stehno, Y. Huang, M. S. Golden, A. A. Golubov, A. Brinkman, and V. S. Khrapai, Andreev reflection in an s-type superconductor proximized 3D topological insulator, *Phys. Rev. Lett.* 117(14), 147001 (2016)

45. J. Wiedenmann, E. Liebhaber, J. Kübert, E. Bocquillon, P. Burset, C. Ames, H. Buhmann, T. M. Klapwijk, and L. W. Molenkamp, Transport spectroscopy of induced superconductivity in the three-dimensional topological insulator HgTe, *Phys. Rev. B* 96(16), 165302 (2017)